Unclassified

LEVEL II

14 AUG 1981

3

AD A105518

DTIC FILE COPY

REPORT DOCUMENTATION PAGE (19)	READ INSTRUCTIONS BEFORE COMPLETING FORM
1. Report Number (18) AFOSR-TR-81-0652	2. Govt Accession No. AD-A105 518	3. Recipient's Catalog Number
4. Title (and Subtitle) (6) LITHIUM BASED ANODES FOR SOLID STATE BATTERIES.	5. Type of Report & Period Covered Final Scientific 1 Jul 77 - 30 Jun 81
	6. Performing Org. Report Number
7. Author(s) (10) R.A.H. Edwards, J.R. Owen and B.C.H. Steele	8. Contract or Grant Number AFOSR-77-3460
9. Performing Organization Name and Address Department of Metallurgy & Materials Science Imperial College of Science & Technology London SW7 2BP, UK	10. Program Element, Project, Task Area & Work Unit Numbers 61102F (12) 2303/A1 (17) A1
11. Controlling Office Name and Address Air Force Office of Scientific Research/NC Bolling AFB Washington, DC 20332	12. Report Date (11) 30 Jun 1981
	13. Number of Pages 38
14. Monitoring Agency Name and Address (14) 9871	15. Unclassified

DTIC ELECTE OCT 0 9 1981 E

16. & 17. Distribution Statement

Approved for public release; distribution unlimited.

18. Supplementary Notes

19. Key Words

SOLID STATE BATTERIES
LITHIUM ANODES
MIXED IONIC AND ELECTRONIC CONDUCTORS
INTERFACIAL STUDIES

20. Abstract

The work of the two previous reports is reviewed and the last year's work is reported in detail. The latter involved the use of "staircase wave cyclic voltammetry," a technique designed to characterize the transport properties of an electrode material over a wide composition range. This technique was applied to the compounds Fe_x^1, Si, a glassy metal of composition $(Fe_{95}Si_7)B_{15}$, and a newly found prospective negative plate material Hg_xLi.

An analysis of composite electrodes - those containing an additional ionic conductor, e.g. a solid electrolyte, as the grain boundary phase of the charge storage material shows that the criteria initially applied to the selection of an electrode may be significantly relaxed. Experiments with the composite of lithium-aluminum alloy with the solid electrolyte polyethylene oxide-lithium trifluoromethane sulphonate have verified the analysis which can be applied to many more systems.

FORM 1473

408846

Unclassified

17

AFOSR-TR- 81 -0652

Grant Number : AFOSR - 77 - 3460

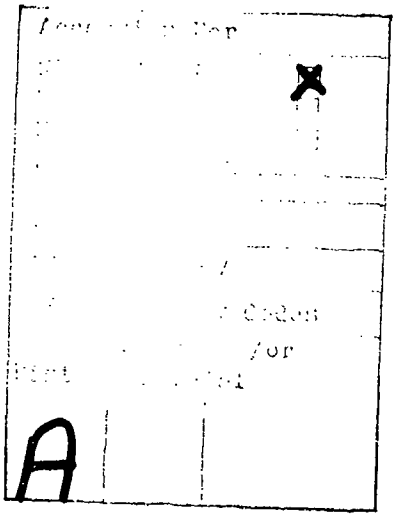

LITHIUM BASED ANODES FOR SOLID STATE BATTERIES

R.A.H. Edwards, J.R. Owen and B.C.H. Steele
Wolfson Unit for Solid State Ionics,
Department of Metallurgy & Materials Science,
Imperial College, London, SW7 2BP.
United Kingdom.

30th June 1981

Final Scientific Report
30th September 1977 - 30th September 1980

Approved for public release; distribution unlimited.

Prepared for:

AFOSR, Bolling AFB, DC 20332

and

European Office of Aerospace Research & Development,
London, England.

CONTENTS

		Page
1.	Introduction.	1
	1.1. Background discussion.	1
	1.2. Summary of work during previous periods.	5
	1.3. Methodology of research during the present period.	6
2.	Staircase wave cyclic voltammetry.	8
	2.1. Principle of the technique.	8
	2.2. Control and analysis by microcomputer.	11
	2.2.1. Control program.	11
	2.2.2. Analysis program.	13
	2.3. Results.	13
	2.3.1. $Fe_{93}Si_7B_{15}$ glassy metal.	14
	2.3.2. $FeSi_2$.	14
	2.3.3. Hg.	14
	2.4. Evaluation of results.	14
3.	Composite electrodes.	19
	3.1. Introduction	19
	3.2. The electrochemical model of the diffusion process.	20
	3.2.1. Insertion of ions into an electrode particle.	21
	3.3. Application to composite electrodes.	21
	3.3.1. σ electrolyte > σ electrode : large grain size.	24
	3.3.2. σ electrolyte > σ electrode : small grain size.	24
	3.3.3. σ electrolyte > σ electrolyte.	24
	3.4. Polyethylene oxide solid electrolytes.	24
	3.5. Composite Li/Al/polyethylene oxide electrodes.	26
4.	Re-appraisal of negative plate materials.	31
5.	Appendix 1.	34

1. Introduction

1.1. Background discussion

A considerable effort has recently been devoted to the production of a rechargeable lithium anode for use in secondary lithium batteries. Three main problems associated with the use of pure lithium as the negative plate are as follows:

(a) Formation of surface films with excessive resistance

Lithium metal reacts with the majority of organic materials used as electrolytes; the reaction is terminated in many cases only by the formation of a passivating surface film of lithium carbonate amongst other compounds. In this case the film resistance can give a significant contribution to the cell "IR" loss during operation.

(b) Isolation of redeposited lithium particles

The passivating film remains on the anode during recharge, and also forms around particles of replated Li and thus at least partially isolating them from the circuit collector. In this case the capacity of the electrode is reduced on each cycle. Although some modifications of the electrolyte composition have proved relatively successful (1) the problems are not yet fully solved and a large excess of lithium is usually used on the negative plate to compensate the capacity loss.

(c) Lithium dendrite cell shorting

The active mass of lithium is geometrically redistributed on each charge/discharge cycle and the most serious consequence of this phenomenon is the growth of lithium dendrites. If a single dendrite penetrates the electrolyte layer during charging and contacts the positive plate, the resulting short circuit permanently disables the cell.

The choice of an alternative negative plate to pure lithium is intended to solve the above problems in two respects. Firstly the activity of lithium, and therefore the tendency for chemical

(1) e.g. S.B. Brummer, Proceedings of the Workshop on Lithium Non aque ous Battery Electrochemistry. Case Western Reserve Univ. June 4-6 1980, pp.130-142, The Electrochemical Soc., Proc. vol. 80-7.

reaction with the electrolyte, is reduced, albeit at the penalty of a reduced cell voltage. Secondly, the immobile host structure provides a geometrical location for the active mass, and any temporary redistribution of lithium is corrected by the thermodynamically driven diffusion of lithium to give a constant composition throughout the host material.

The most common example of the use of a lithium compound as the negative plate material is the case of the lithium aluminium system. The electrochemical phase diagram of this system is shown in fig. 1, which shows the thermodynamic e.m.f. value of the alloy versus a lithium electrode as a function of the lithium composition.

The phase diagram shows that the useful range of lithium insertion includes at least three phase modifications of the alloy. The two-phase regions are undesirable in that they involve a rather excessive volume change and that the nucleation and growth of the new phase during charge or discharge involves an additional kinetic limitation. From this point of view the Li_xMg system is preferable, in that it shows a wide single phase solid solution region (fig. 2).

Lithium alloys have been used as the negative plate material in fused salt batteries (2) and in liquid organic electrolyte batteries (3). In both cases structural changes in the electrode due to crystallographic phase change were acceptable because of the penetration of liquid electrolyte into the grain boundary regions. However, this cannot occur in the case of the solid state battery where the mass transport within the electrode phase occurs by diffusion. Accordingly, the major effort in the present study was to characterise the solid state diffusion within selected lithium alloys in order to predict their performance as negative electrodes.

(2) e.g. Tomczuk et al, J. Electrochem. Soc. 127, (80)1981.

(3) Garreau et al Ref. 1.

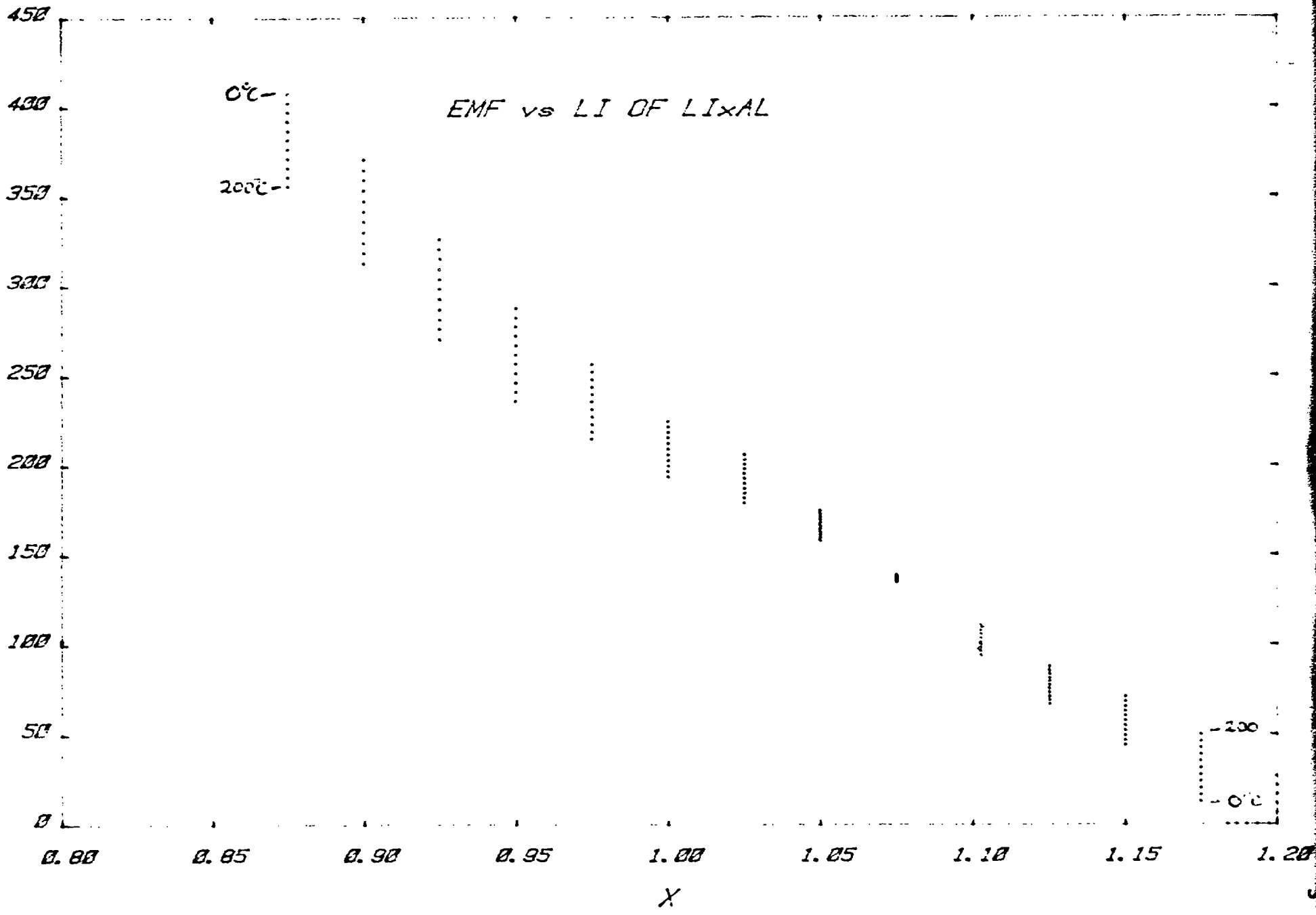

Fig 1 E.m.f. of Li x Al at various temperatures.

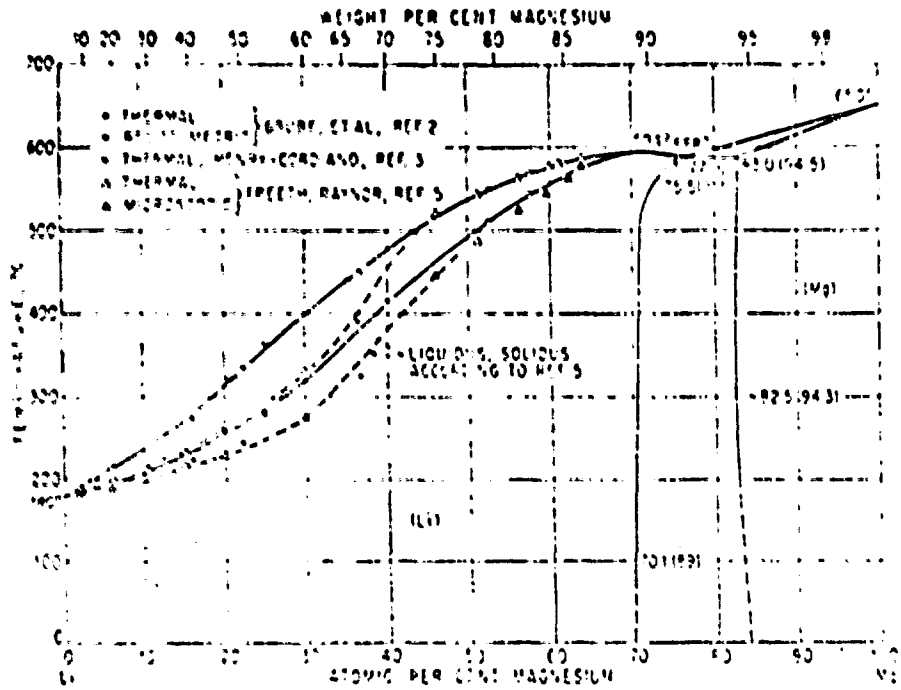

Fig. 2. Li-Mg phase diagram showing wide solid solution region. (from M. Hansen, "Constitution of Binary Alloys", McGraw Hill, 1958).

1.2. Summary of work during previous periods.

The first project period began with the identification of the requirements of the insertion material. Apart from the more obvious requirements of a large composition range and a high value of the chemical diffusion coefficient, $\tilde{D}_{Li}$, over a suitable voltage range with respect to lithium the application in a solid state battery required a consideration of the stability of the interface with a solid electrolyte and the kinetics of ion transfer across this interface.

A preliminary survey of the use of lithium alloys in fused salt and liquid organic electrolytes showed that most of the alloys with higher diffusion coefficients underwent phase changes upon lithium insertion. The interface with a hard solid electrolyte was not expected to withstand the severe dimensional changes involved, and accordingly the useful stoichiometric range corresponding to single phase existence was too narrow to give an acceptable energy density. The compounds $Li_xFe_ySi_2$ and $Li_4Mn_4P_4$ were chosen for study on structural grounds; both materials were known to have highly defective structures and were then expected to show fast lithium diffusion. Samples of the former were made and hot-pressed into electrodes but the latter was found to be too moisture sensitive for study. $Li_xFe_ySi_2$ was tested in a solid state cell involving the glassy electrolyte $Li_{3.6}Si_{0.6}P_{0.4}O_4$ and a Li_xTiS_2 counterelectrode and reference electrode. E.m.f. values were found to be similar to those reported for Li_xAl and preliminary estimations of the diffusion coefficient were encouraging.

Interfacial studies indicated favourable properties of the novel polymeric electrolytes based on lithium salt complexes with polyethylene-oxide (4). The mechanical deformability of the electrolyte aided the fabrication of an intimate solid contact essential for the study of kinetic parameters.

During the second period work continued on the $Li_xFe_ySi_2$ system and also included some other lithium alloys. Fe_xSi_2 was found to form the desired alpha phase at the compositions with 70 to 72.5

(4) M.B. Armand et al "Fast Ion Transport in Solids", eds. Vashishta, Mundy and Shenoy, (North Holland, 1979).

atomic per cent Si. The other materials examined were Al foil, Pd/Y foil (previously found to be a good material for hydrogen insertion), and 2826 MB glassy metal (Allied Chemicals). Pt foil, Ni foil and TiS_2, VSe_2, respectively were used as inert and active electrochemical standards.

Initial cyclic voltammetry experiments using solutions of lithium perchlorate in propylene carbonate as the electrolyte gave erratic results due to mechanical instability of the electrodes. An improved cell design incorporated a porous separator of polyvinyl chloride. Electrochemical techniques used were cyclic voltammetry, potential step amperometry and galvanostatic step potentiometry. These experiments were intended as a screening technique for new materials rather than a detailed investigation of the diffusional properties as a function of composition. Accordingly, a figure of merit was defined as the average value of $D\ (\Delta x)^2$ over a given potential range, where Δx was the compositional change caused by a potential step across the range. (This figure is directly related to the rate of discharge or charge under potentiostatic conditions and was therefore an appropriate kinetic figure of merit). The $FeSi_2$ samples showed the most promising results with $D\ (\Delta x)^2$ values of about 5×10^{-11} $cm^2 sec^{-1}$ at the best composition, which was surprisingly found to be in the high silicon two phase region. This figure of merit was about one order of magnitude below the corresponding value for one of the best known positive insertion electrodes, TiS_2.

Detailed accounts of the above work are given in the two interim scientific reports for 1977/78 and 1978/79.

1.3. Methodology of research during the present period

In the previous phase of the project the kinetics of lithium insertion into a given material were described by the single figure of merit $D\ (\Delta x)^2$, applied for a defined, large voltage step ΔV. However, a more detailed examination is required to establish the electrode's kinetic activity as a function of potential. Cyclic voltammetry at a very slow scan rate can be used to determine the thermodynamic V/x relationship but gives no kinetic information. The method used here and to be described in the next section combines the slow scan voltammogram with the potential step method and thus provides more complete information on the insertion re-

actions. It will be shown later how the E-x and $D(\frac{dE}{dx})^{-2}$ data can be used to predict the electrode's energy and power density respectively.

Since the electrode material will be used eventually as a polycrystalline agglomerate, probably of quite small grain size, the simple diffusion theory of a single phase material has to be modified to take into account the grain boundaries, which will have a different value of diffusion coefficient to the bulk material. Although the thermodynamic properties of the electrode are usually independent of the grain boundary properties the kinetics of electrode cycling can often be dominated by transport in grain boundaries; it is therefore essential to develop a composite theory of mass transport involving both bulk and grain boundary parameters. Such a theory is outlined in the penultimate section of this report.

Finally two new materials have been designed on the basis of the composite diffusion theory. These are the composites of LiAl with mercury and polyethylene oxide trifluoromethane sulphonate. The respective additives to LiAl are used as grain boundary phase ionic conductors to feed small grains of LiAl which is the charge storage medium. The thermodynamic properties of LiAl are well known and the transport properties of the grain boundary phases, polyethylene oxide trifluoromethane sulphonate and lithium mercury alloy were determined. The composite electrode with the polymeric grain boundary material has been successfully made and used in a solid state battery.

2. Staircase wave cyclic voltammetry

2.1. Principle of the technique

Cyclic voltammetry has been used in the preliminary screening and in the detailed assessment of insertion electrode materials. In the latter case the scan rate required is extremely slow, the scan time being proportional to the square of the electrode thickness; and only the thermodynamic properties are given as a result.

Potential step chronoamperometry may be used to evaluate the kinetic properties of a sample, and in contrast to the large steps used in the application of this technique for preliminary screening, small potential steps must be used to obtain accurate diffusion data. A series of such small potential step experiments is required to fully characterise a sample. The staircase wave cyclic voltammetry used here is a combination of the two methods above. The cyclic voltammogram is performed slowly and stepwise; the charge passed during each step has the same significance as the average current at the same voltage range in a normal cyclic voltammogram. The current passing during each step must then be integrated to give the charge, which, the limit of zero scan rate, may be related to the composition change due to the voltage step. The transient current response to each step can be analysed to give the diffusion coefficient in the same way as in potential step chronoamperometry. In the first approximation the current is initially limited by resistance effects but as the diffusion becomes the limiting factor the current decays according to the Cottrell $t^{-\frac{1}{2}}$ law:

$$\frac{I}{A} = F\left(\frac{\tilde{D}}{\pi}\right)^{1/2} \cdot \left(\frac{\Delta x}{V_m}\right) t^{-1/2}$$

where F = Faraday's constant , V_m = molar volume

$\left(\frac{\Delta x}{V_m}\right)$ = concentration change caused by voltage step $= \Delta c$

or in terms of the voltage this is

$$\frac{I}{A} = \frac{F}{V_m}\left(\frac{\tilde{D}\left(\frac{dE}{dx}\right)^{-2}}{\pi}\right)^{1/2} \Delta E \cdot t^{-1/2}$$

where $\frac{dE}{dx}$ is slope of E.M.F./composition curve

ΔE = applied voltage step.

The material parameter directly measured is thus the quantity, $D(\frac{dE}{dx})^{-2}$. This may be considered as a figure of merit at the particular composition, it also indicates the overpotential produced on constant current drain

$$V = \frac{2}{F} \cdot \frac{I}{A} \cdot \frac{1}{(\pi D)^{1/2}} \left(\frac{dE}{dc}\right) t^{1/2}$$

The $t^{-\frac{1}{2}}$ behaviour above is theoretically derived for a specimen of infinite length. For finite length samples $t^{-\frac{1}{2}}$ behaviour continues for a time $\tau \approx \frac{L^2}{D}$, then the current decays exponentially to zero as thermodynamic equilibrium is approached.

For most of the samples used, $\frac{L^2}{D}$ was quite long (at least four hours) and therefore it was not possible to wait for the expotential decay region after each step. Therefore only the first voltage step could be expected to obey the Cottrell Law. Subsequent voltage steps should show Cottrell currents superimposed on the residual currents from the previous steps as shown in fig (3). Although the additivity of the various Cottrell currents from many potential steps to give the actual circuit may be intuitively expected, the mathematical proof is complex, and is given in appendix 1.

The electrochemical cell and associated circuitry used for the staircase wave cyclic voltammetry are shown in fig. (4). A Commodore PET microcomputer with DAC and ADC interfaces was used to program the potentiostat and to record the current values. Typically the current was sampled at 10sec intervals and recorded for a voltage cycle form zero to one volt vs. a Li reference in 100mV steps regularly spaced at one hour intervals. For each voltage step the current was plotted versus time on a video display and was observed to be of the form shown in fig. (3). On playing back the recorded results a correction was applied to the current values in order to separate the $t^{-\frac{1}{2}}$ contributions due to each voltage step.

The staircase wave voltage signal may be expressed thus:

$$V(n) = V(n-1) + S \qquad \text{where } n = \text{step number}, \quad S = \text{step height}$$

Typically, a 2 volt range was covered in 100mV steps equally spaced about one hour apart. At the specified maximum and minimum potentials of the range the sign of S was changed giving an approximately

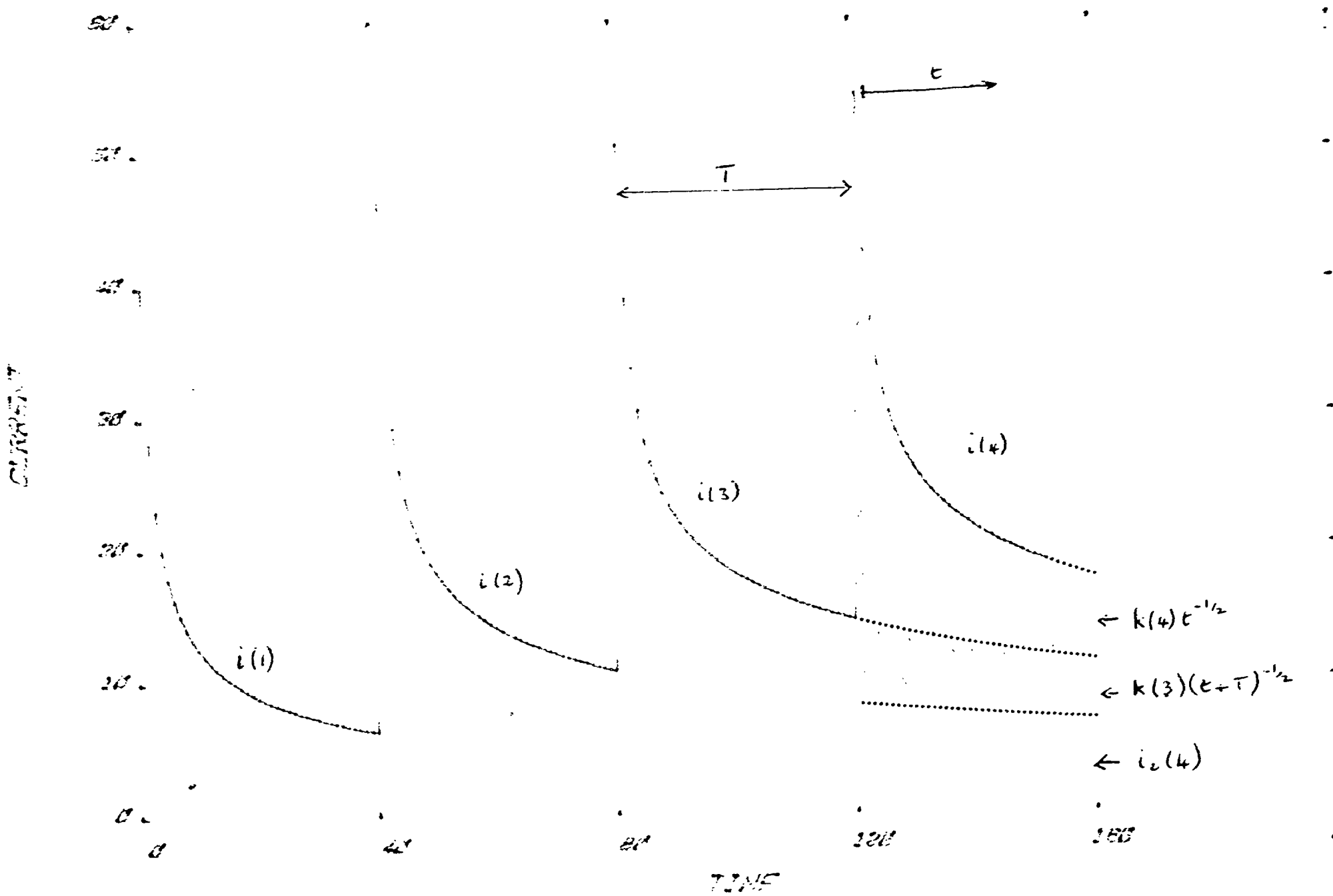

Fig 3. Simulated response to staircase voltage

triangular cyclic voltammogram (fig. 5). The current during the n^{th} step was considered to be of the form:

$$i(n) = i_o(n) + k(n-1)(t+T)^{-\frac{1}{2}} + k(n)t^{-\frac{1}{2}}$$

where T = step duration

t = time elapaed after the voltage was changed.

The residual current from the previous step was accounted for as a time dependent current, $k(n-1)(t+T)^{-\frac{1}{2}}$, whereas the residuals from earlier steps were grouped together as a time independent background current, $i_o(n)$. The first step was of Cottrell form, with $i_o(1) = 0$ and $k(o) = 0$, and the gradient $di(1)/dt^{-\frac{1}{2}}$ yielded a value of k(1). This value was then used to correct the current values during the second step, subtracting $k(1)\ (t+T)^{-\frac{1}{2}}$ from each value before the Cottrell analysis which then yielded k(2). In subsequent steps the corrected Cottrell plot gave positive values of the intercepts, $i_o(n)$ due to the combined contributions of previous steps. The result was a histogram of the values of k(n) versus the potential, V(n). The significance of the histogram towards predicting power density will be discussed in the final section.

2.2. Control and analysis by microcomputer

The following notes describe the use of the Commodore PET microcomputer for the voltage programming, current recording and analyser of results.

2.2.1. Control program

(a) Program inputs the following quantities form the key board:
- initial potential (mV)
- step height (mV)
- ramp rate (mV per day)
- lower potential limit (mV)
- upper potential limit (mV)
- number of reversals of the voltage sweep
- specimen details text.

(b) Program waits for a keyboard start command then outputs the initial potential plus the specified step to the potentiostat.

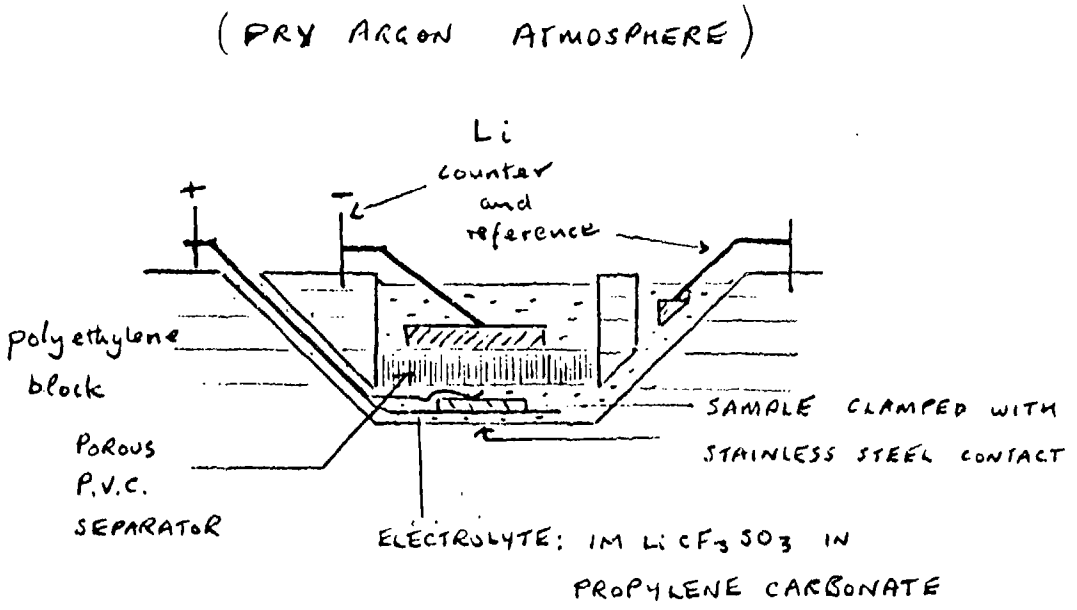

Fig. 4 - ELECTROCHEMICAL CELL

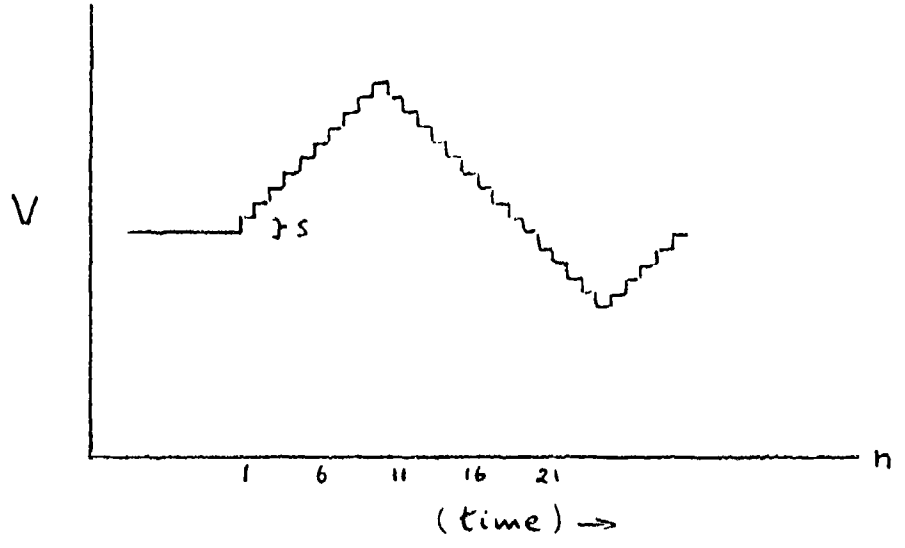

Fig. 5 - STAIRCASE POTENTIAL

(c) Program calculates the required duration of each voltage step and divides this period into forty time intervals.

(d) During each time interval above the current reading is interrogated every second and averaged over the interval. The averaged currents for each of the forty intervals are plotted on the screen to show the current decay.

(e) At the end of each step the current values are recorded on a cassette tape. The potential value of the next step is calculated according to the step height, limits and number of reversals required.

(f) Program stops after the last reversal.

2.2.2. Analysis program.

(a) Program reads and displays the quantities input in (a) above.

(b) Program displays the potential, forty current values and their sum which corresponds to the total charge passed.

(c) Program calculates correction currents based on previous step and subtracts from each current value (this is omitted on the first step). (A keyboard command may suppress the correction if required).

(d) Program displays a graph of current and (corrected current)$^{-2}$ versus time.

(e) For each consecutive pair of currents, program calculates the gradient $dI/dt^{-\frac{1}{2}}$.

(f) Program calculates the average gradient, ignoring values of more than 15% variance.

(g) Program calculates the intercept and subtracts from each current value.

(h) Program displays corrected Cottrell graph and the value of k.

(i) Program returns to (b) for results of next step.

2.3. Results

2.3.1. $Fe_{93}Si_7B_{15}$ glassy metal

Fig (6) shows histograms of the differential capacity (charges obtained by summation of uncorrected currents) and $D^{\frac{1}{2}}(dE/dc)^{-1}$ values obtained from the correction procedure. (The differential capacity values represent the information normally given by a cyclic voltammogram). Comparison of the two graphs shows the superior resolution of the correction procedure; the corrected graph shows electrochemical activity peaks at 800mV and 1300mV versus lithium.

Fig. (7) shows the same analysis on the glassy metal after sputter etching and platinum coating to eliminate surface oxidation; the result was similar to the untreated sample.

2.3.2. $FeSi_2$

Fig (8) shows the values of $D^{\frac{1}{2}}(\frac{dE}{dx})^{-1}$. The figure of merit varies smoothly with potential, and is about one order of magnitude larger than that of the glassy metal in the region up to 500mV versus lithium.

2.3.3. Hg

Specimens of the lithium amalgam were prepared by dissolving freshly cleaned lithium metal in mercury. In this case the figure of merit was large in the regions below 200mV and above 800mV.(fig 9).

2.4. Evaluation of results.

The glassy metal sample showed very little lithium insertion and can be ruled out as a negative plate material. $FeSi_2$ was more encouraging, but the values of the figure of merit are still too low for the material to be of practical use. The amalgam samples, however, were very encouraging. The high lithium mobility below 200mV was attributed to the phase Li_3Hg and other phases higher in lithium content. At intermediate potentials the mobility is severely decreased but a strong activity is shown again above 800mV, probably corresponding to the formation of a liquid amalgam from $LiHg_3$.

Because of the high density of mercury and the formation of liquid amalgam the Hg/Li system cannot be used alone as a negative plate material. However, it will be shown in the next section that HgLi may form the lithium transporting agent of a composite

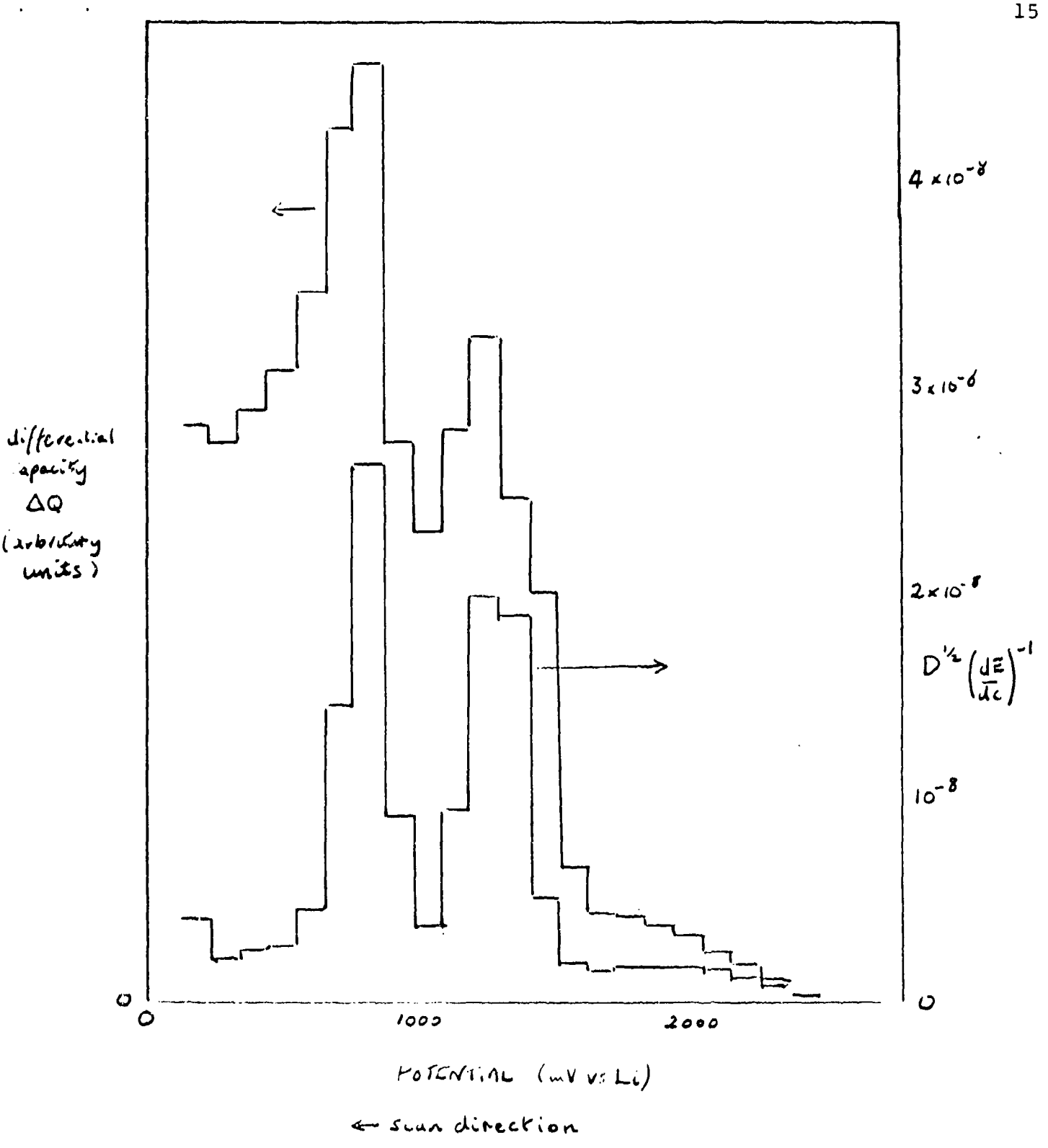

Fig. 6 Comparison of cyclic voltammetric analysis (upper) with corrected analysis (lower) for $Fe_{93}Si_7B_{15}$ glass

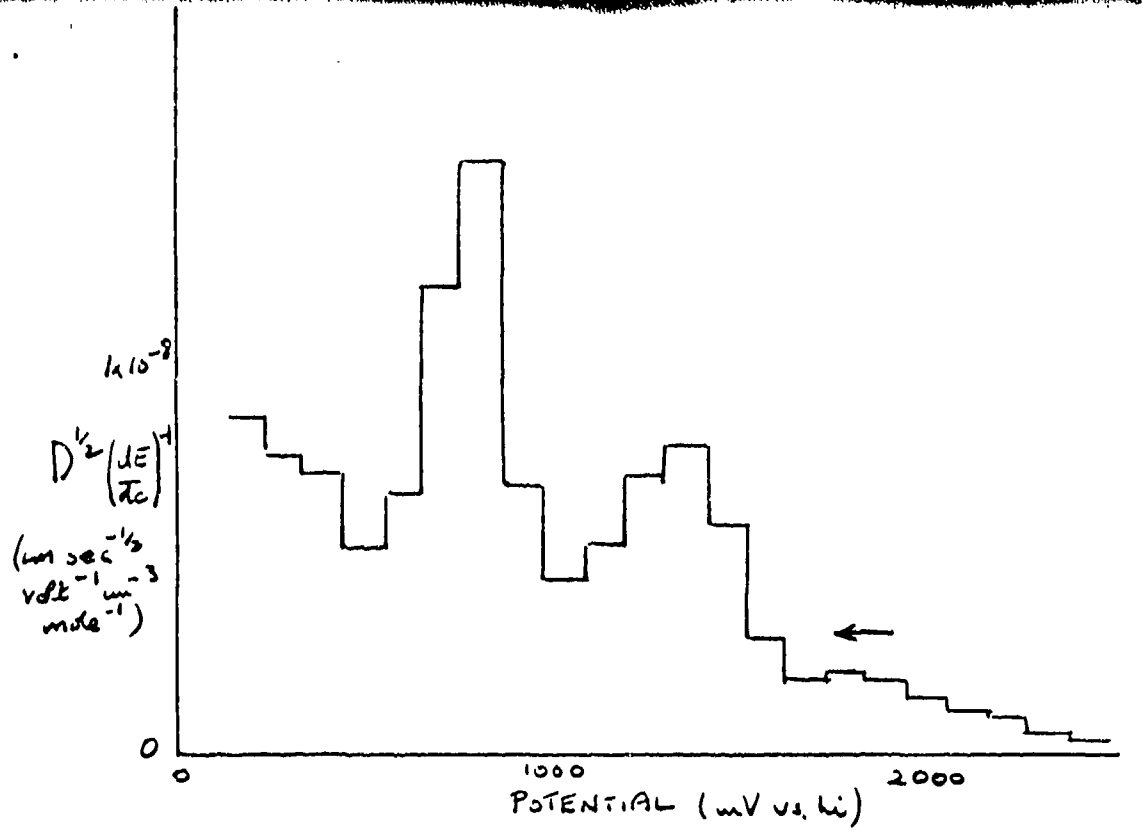

Fig. 7. Analysis of iron-etched $Fe_{93}Si_7B_{15}$

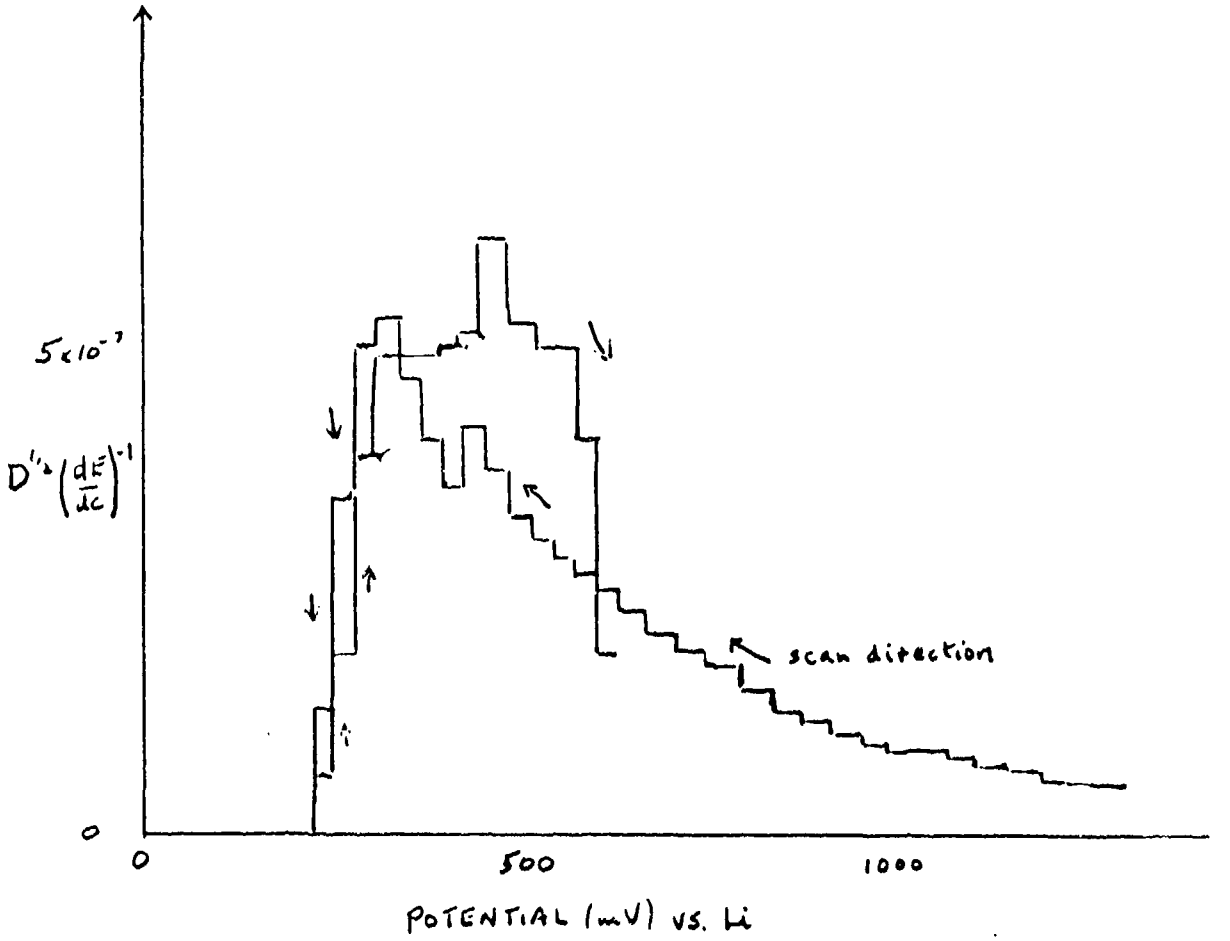

Fig. 8. Analysis of $FeSi_2$

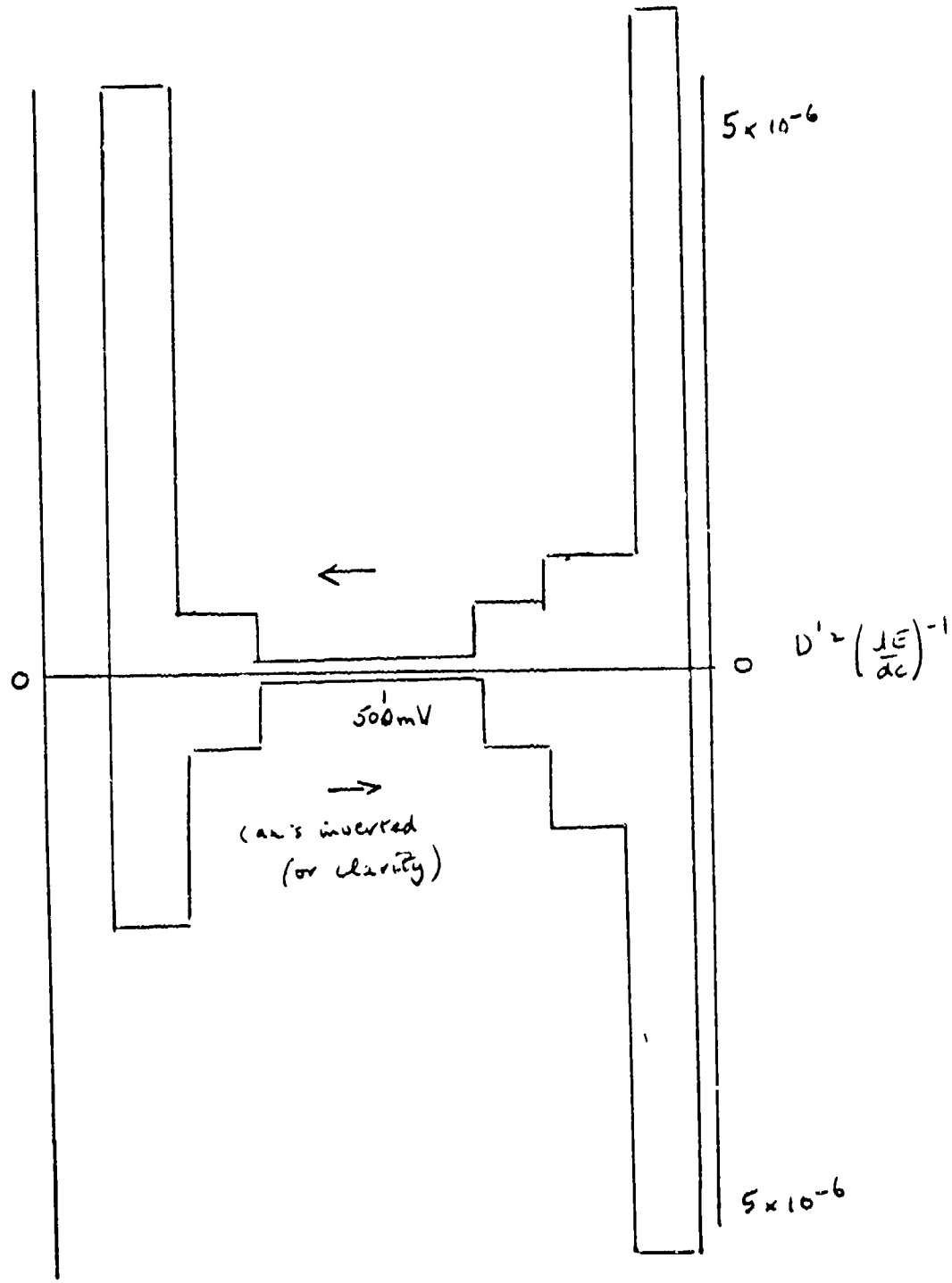

Fig. 9 Analysis of HgCdTe

material to be used as a negative plate.

3. Composite electrodes

3.1.

The term "composite electrode" is used here to describe an agglomeration of small grains of an insertion electrode material bound together by another phase, usually but not necessarily a soft solid electrolyte, and may therefore be applied to all situations where an insertion electrode is used in polycrystalline form. In the simplest treatment, electronic conduction is assumed to be unrestricted even at interparticle contacts so that ionic conduction through the intergrain phase will play the major role in ensuring continuity of the mass transport route.

The composite electrode is thus the solid state analogue of the porous electrode used in liquid electrolyte batteries, however, here are four important differences in the electrochemical analysis:

(a) The insertion electrode material itself may, in some cases, transport the electroactive ions as effectively as the electrolyte, which is generally a poorer conductor than its liquid counterpart.

(b) The composition of the insertion electrode varies within the grains and the consequent variation of the surface redox potential is a major contribution to the cell overpotential.

(c) The composition of the electrolyte is generally regarded as constant, in which case there is no concentration overpotential in the electrolyte.

(d) The activation barrier against the ion passing between two phases is of a different nature to that encoutered in interfaces where a new phase is grown, and the impedance arising from the barrier may be less important in the former case.

Current research on materials for advanced batteries is distributed between studies of transport in electrolytes, electrodes and their interfaces, and in order to be able to judge how much emphasis should be placed on each aspect, the rate limiting steps should be clearly identified. An unfortunate complication of many transport calculations is the formulation of equations simultaneously involving Fick's law and Ohm's law with the result that the overall situation is difficult to visulize. A simplification is

achieved below by obtaining the ionic conductivity of the insertion electrode from its diffusion coefficient thereby expressing Fick's law in a more useful form.

3.2. The electrochemical model of the diffusion process

The properties of an insertion electrode are usually described in terms of the chemical diffusion coefficient, $\tilde{D}$, thermodynamic factor, $d\ell na/d\ell nc$, and the open circuit electrode potential, E, as a function of the guest ion concentration, c (mole cm^{-3}):

$$\frac{d\ell na}{d\ell nc} = \frac{d\mu(M^+)}{d\ell nc} \cdot \frac{1}{RT}$$ where $\mu(M^+)$ is the chemical potential of the neutralized inserted ion, M^{z+}

$$= \frac{-zFc}{RT} \cdot \frac{dE}{dc}$$

The Nernst-Einstein equation relates the self-diffusion coefficient, D, to the ionic conductivity, writing this in molar units we have:

$$\sigma = \frac{cDz^2F^2}{RT}$$, and since the chemical diffusion coefficient, $\tilde{D}$ is usually equal to $D.d\ell n\ a/d\ell n\ c$ we obtain,

$$\sigma = -zF(dE/dc)^{-1}.\tilde{D} = -k\tilde{D}$$

k is the electrolytic capacitance per unit volume whose inverse is demonstrated by the rate of change of electrode potential with applied ionic current (balanced by an equal electronic current preserving bulk charge neutrality): for a small volume, δV, Faraday's law gives:

$$I(e^-) = I(M^+) = zF\delta V\ dc/dt = zF\delta V\ (dE/dc)^{-1}\frac{dE}{dt}$$

$$= -k\delta V\ dE/dt$$

(Since $\sigma/k = -\tilde{D}$ and $\sigma\ k = \tilde{D}zF(dE/dc)^{-2}$, σ and k may be easily found experimentally e.g. by coulometric titration). Rather than applying Fick's law to the transport of ions in the electrode, the ionic current density, $J(M^+)$ may be seen as the response to the electrochemical potential gradient, according to the Nernst-Planck equation:

$$J(M^+) = -\sigma(M^+).d\tilde{E}(M^+)/dy \qquad \ldots.(1)$$

where $\tilde{E}(M^+)$ is the electrochemical potential of M^+ expressed in volts, $\tilde{E}(M^+) = \tilde{\mu}(M^+)/zF$ and similarly, for electrons,

$$J(e^-) = -\sigma(e^-).d\tilde{E}(e^-)/dy \qquad \ldots\ldots(2)$$

The electrolytic capacitance per unit volume, k is seen as a continuous source or sink for ionic and electronic current according to

$$\Delta I(e^-) = \Delta I(M^+) = k\delta V\, dE/dt$$

$$= -k\delta V\, d/dt\, \{E(M^+) + E(e^-)\} \quad \text{or}$$

$$\Delta J(e^-) = \Delta J(M^+) = -k\delta y d(\tilde{E}(M^+) + \tilde{E}(e^-))/dt \qquad \ldots.(3)$$

where it is realized that the electrode potential, E, is the negative sum of the ionic and electronic electrochemical potentials. The equations (1) to (3) are illustrated by the network of fig.10 and an analysis similar to that of de Levie gives:

$d^2E/dy^2 - \{\rho(M^+) + \rho(e^-)\}\ j\omega kE = 0$ where $\rho = 1/\sigma(j\omega k$ is the admittance per unit volume given by the electrolytic capacitance at angular frequency, ω). Although the equation is equivalent to Fick's law it may be applied to some cases of pseudo diffusional behaviour in which diffusion coefficients are not normally defined.

3.2.1. Insertion of ions into an electrode particle

Referring to fig. 11 the assumption of infinite electronic conductivity leads to the following expression of the impedance at angular frequency ω

$$ZA = \rho(M^+)\ \lambda\coth(L/\lambda) \text{ where } \lambda = (j\omega k\rho(M^+))^{-\frac{1}{2}} \qquad \ldots.(4)$$

For a small penetration depth (λ) of the electrochemical disturbance we obtain the Warburg impedance:

$$ZA = (j\omega k\sigma\ (M^+)^{-\frac{1}{2}}$$

$$= (1-j)\ (2\tilde{D})^{-\frac{1}{2}}\ (dE/dc)\omega^{-\frac{1}{2}}$$

whereas for a large penetration we obtain the equivalent of a resistance and capacitance in series

$$ZA = (j\omega kL)^{-1} + L/3\sigma(M^+)$$

3.3. Application to composite electrodes

The complete description of the interaction between an insertion electrode particle and the electrolyte matrix is approximated by discrete components in fig.12. According to the relative ionic conductivities of the electrode and electrolyte the model simpli-

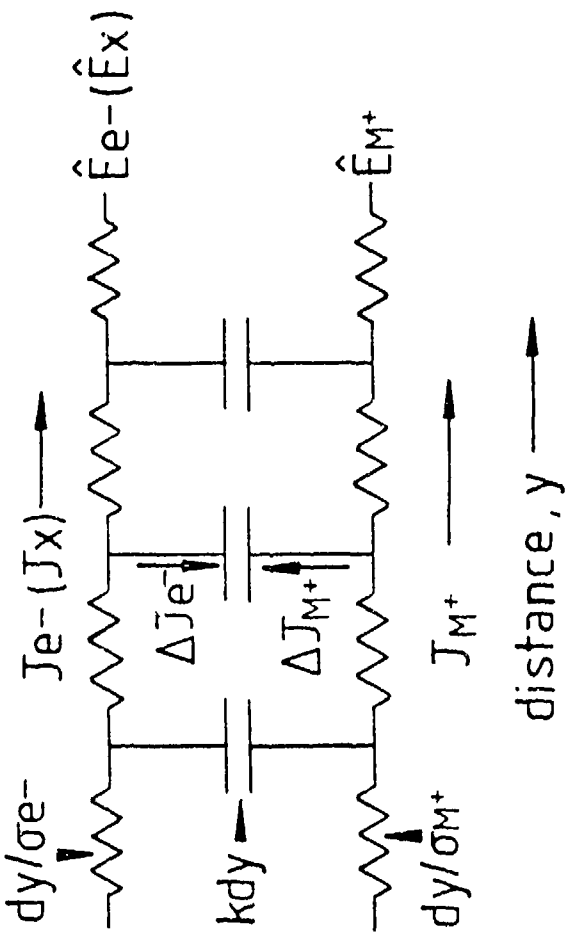

Fig. 10. Electrochemical model of diffusion within electrode material.

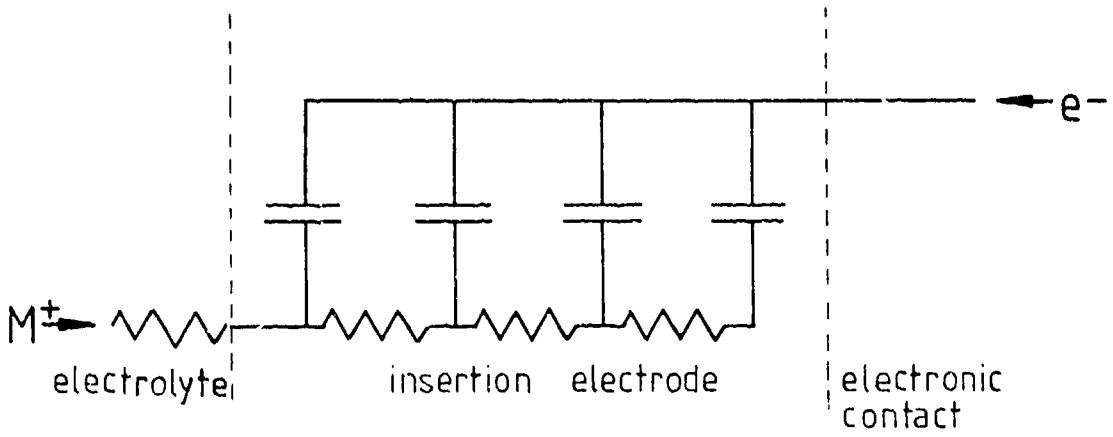

Fig. 11. Insertion of ions into the electrode.

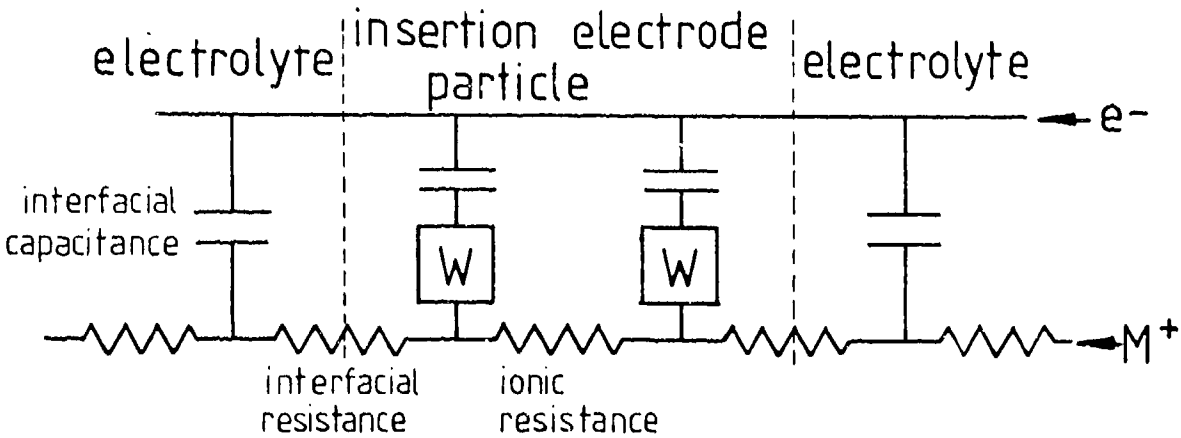

Fig. 12. Interaction of electrode with electrolyte within composite material.

fies as in the following examples. In each case the impedance $Z(\omega^{-n})$ gives rise to a time domain response to a galvanostatic step of $V(t^n)$.

3.3.1. σ electrolyte >σ electrode: large grain size.

In this case the large conductivity of the electrolyte enhances the effective surface area of the electrode within the penetration depth shown in fig. 13(a). The solution is an impedance proportional to $\omega^{-\frac{1}{4}}$ at large ω but as the penetration depth reaches the end of the electrode we obtain:

$$ZA = S\{\rho(M^+)\ \lambda\ \coth\ (L/\lambda)\}$$

(where S is the surface area enhancement factor) which shows the Warburg impedance followed by capacitive behaviour at small ω.

3.3.2. σ electrolyte > σ electrode: small grain size.

The $\omega^{-\frac{1}{4}}$ behaviour above degenerates into $\omega^{-\frac{1}{2}}$ as the penetration depth into the grain approaches the grain size. The grain is then a simple capacitance which may be added to a significant interfacial (e.g. double layer or adsorption) capacitance (fig 13(b)). The $\omega^{-\frac{1}{2}}$ behaviour appears as a diffusional process, although the origin of the "diffusion coefficient" is not diffusional.

3.3.3. σ electrode > σ electrolyte

Electrolyte is added to the insertion electrode compact, if at all, to fill in voids between particles. The limiting resistance is at the grain boundaries as in fig.13(c). Again we obtain $\omega^{-\frac{1}{2}}$ behaviour which is not correctly interpreted by a simple diffusion coefficient.

3.4. Polyethylene oxide solid electrolytes

Following the work of Armand (4) a series of doped polyethylene oxide (mol. wt. $\approx$ 5 million) samples was made using lithium trifluoromethane sulphonate as the ionic dopant. Weighed quantities of polyethylene oxide (B.D.H. chemicals) and the dry salt were dissolved in acetonitrile to give a 2% strength solution. The solution was poured into a glass petri dish (previously coated with a

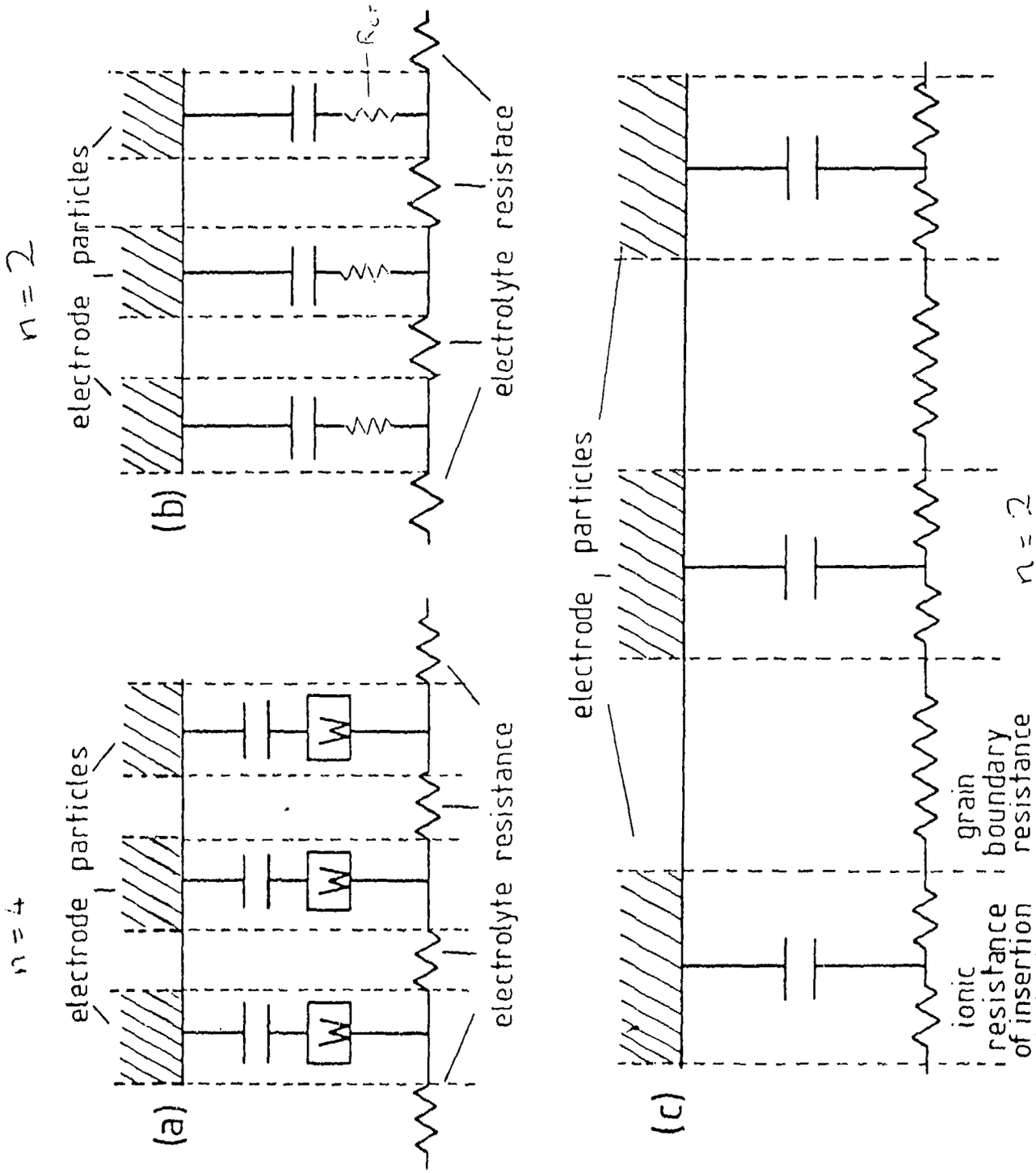

Fig. 13. Models of composite electrodes.

dichlorosilane release agent) to a depth of 5mm, so that the solvent evaporated to leave a 100 micron film. The film was dried at 150°C in vacuo for 24 hours then its conductivity was measured by the A.C. impedance technique using blocking electrodes of stainless steel and an argon atmosphere. The conductivity was measured as a function of composition and temperature; for 120° operation the optimum composition was found to be $(PEO)_8 LiCF_3SO_3$, at which the conductivity was approximately 5×10^{-4} S cm^{-1}.

Optical microscopy showed the films to have a two phase structure at elevated temperatures, containing spherulitic crystals and amorphous grain boundary regions which expanded with increasing temperature as the spherulites gradually disappeared.

The combination of pliability and durability of the polymer films was almost ideal both for the application as the electrolyte membrane and as the ionic conductor in composite electrodes, to be described below.

3.5. Composite Li/Al/polyethylene oxide electrodes

LiAl powder of about 50 micron particle size was obtained from Foote Mineral Company. Because of its pyrophoric nature this material was handled in an argon dry box containing less than 10ppm water. Small quantities of LiAl and $(PEO)_8LiCF_3SO_3$ were weighed to give mixtures at 15, 35, 45 and 55% volume of polymer respectively. Each mixture was homogenized by adding a little acetonitrile (dried over calcium hydride), to dissolve the polymer and grinding in an agate pestle and mortar while the solvent dried. Pellets measuring approximately 6mm diameter, 5mm thick were made at each composition, by cold pressing at pressures between 5 and 20 tonne cm^{-2}. Measurements of the density were within 5% of the theoretical values for samples pressed at pressures above 10 tonne cm^{-2}. The electronic conductivity was measured by a 2-point probe, checking for contact effects by current reversal. Although there were some anomalous results attributed to the presence of some surface oxide films, the conductivity generally followed the predictions of simple percolation theory; thus the conductivity was almost constant up to about 35% volume of polymer and was then seen to fall off sharply as the LiAl particles began to be separated by the polymer.

Taking the polymer conductivity to be about 5×10^{-4} S cm^{-1} at

120°C, the effective ionic conductivity allowing for tortuosity effects in the composite is expected to be about 1×10^{-4} S cm^{-1}. In that case the electronic conductivity of at least 10^{-1} S cm^{-1} up to the composition 45% PEO should not limit the overall transport within the composite electrode.

Some preliminary solid state electrochemical measurements were made using the cell shown in fig 14. Lithium was plated in-situ onto the nickel wire which subsequently functioned as a reference electrode. A partial discharge curve at constant current for the 15% composite is shown in fig. 15. It may be seen that discharge was satisfactory for the initial period where the rate of rise of overpotential decreased with time; however in a later phase the rate of rise of overpotential began to increase, showing a limiting current effect. This effect is not yet fully understood but may be tentatively attributed to a slow diffusion of Li through a compact surface layer of α-Al which may be formed during discharge.

A.C. impedance analysis of the same cell is shown in fig.16. The $\omega^{-\frac{1}{4}}$ impedance indicates that diffusion in the grains is a limiting factor as well as the electrolyte conductivity. Improvements in performance may then be expected by both decreasing the particle size and increasing the polymer electrolyte fraction.

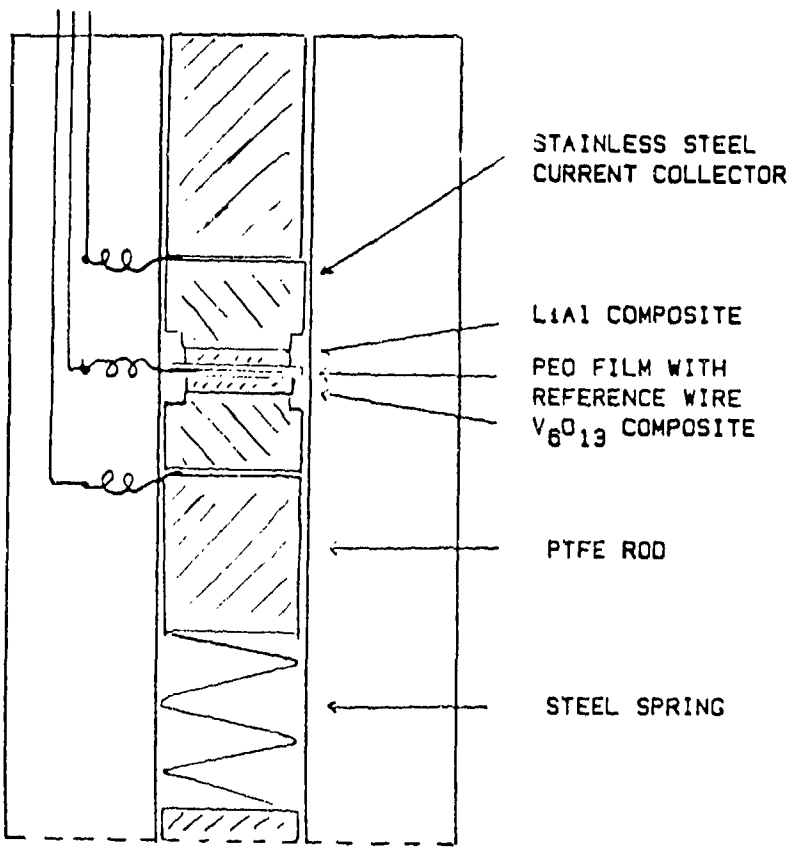

Fig. 14. Solid state cell using LiAl composite.

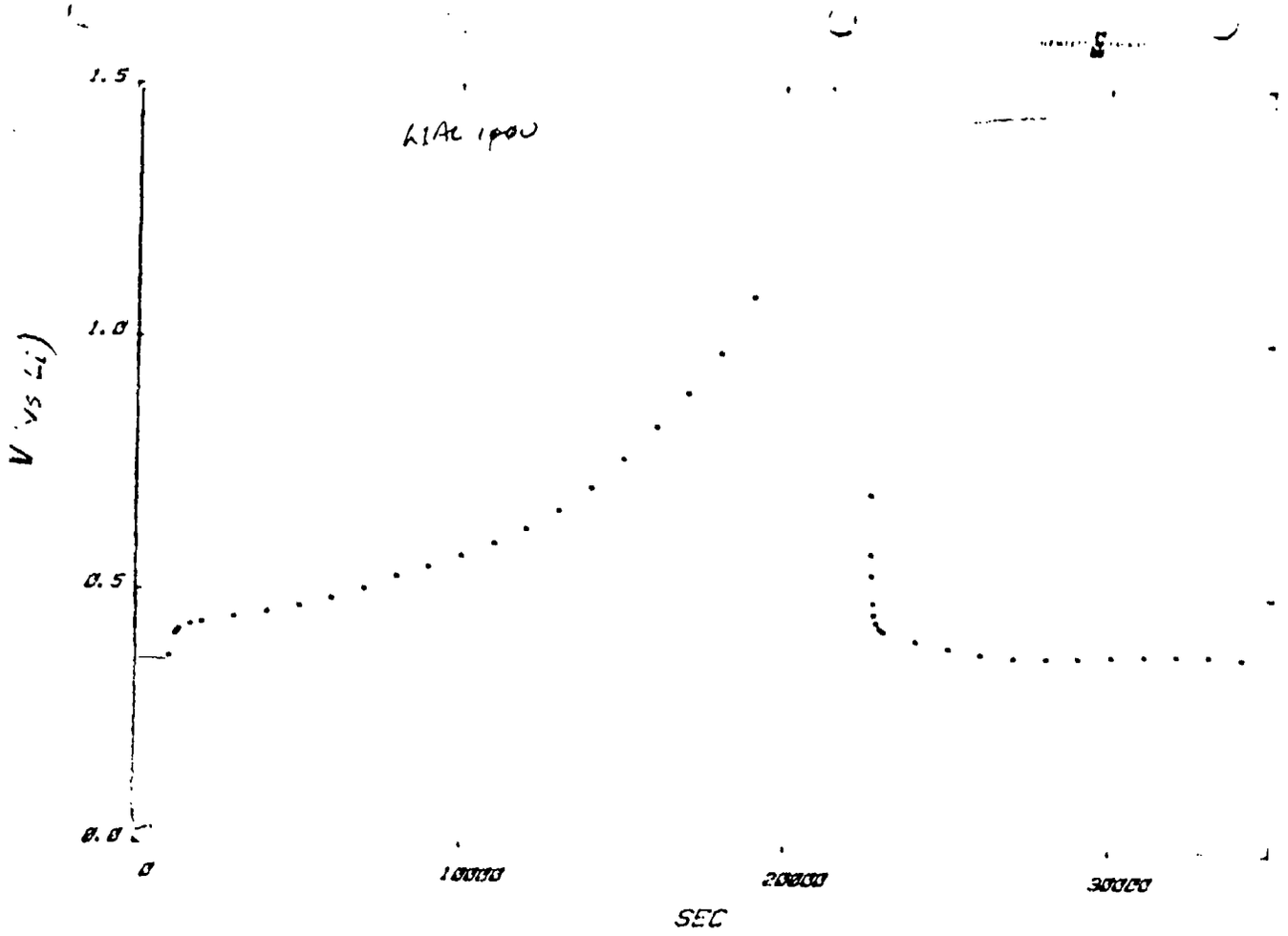

Fig. 15. Potential of LiAl during discharge at 100 microamp cm^{-2}

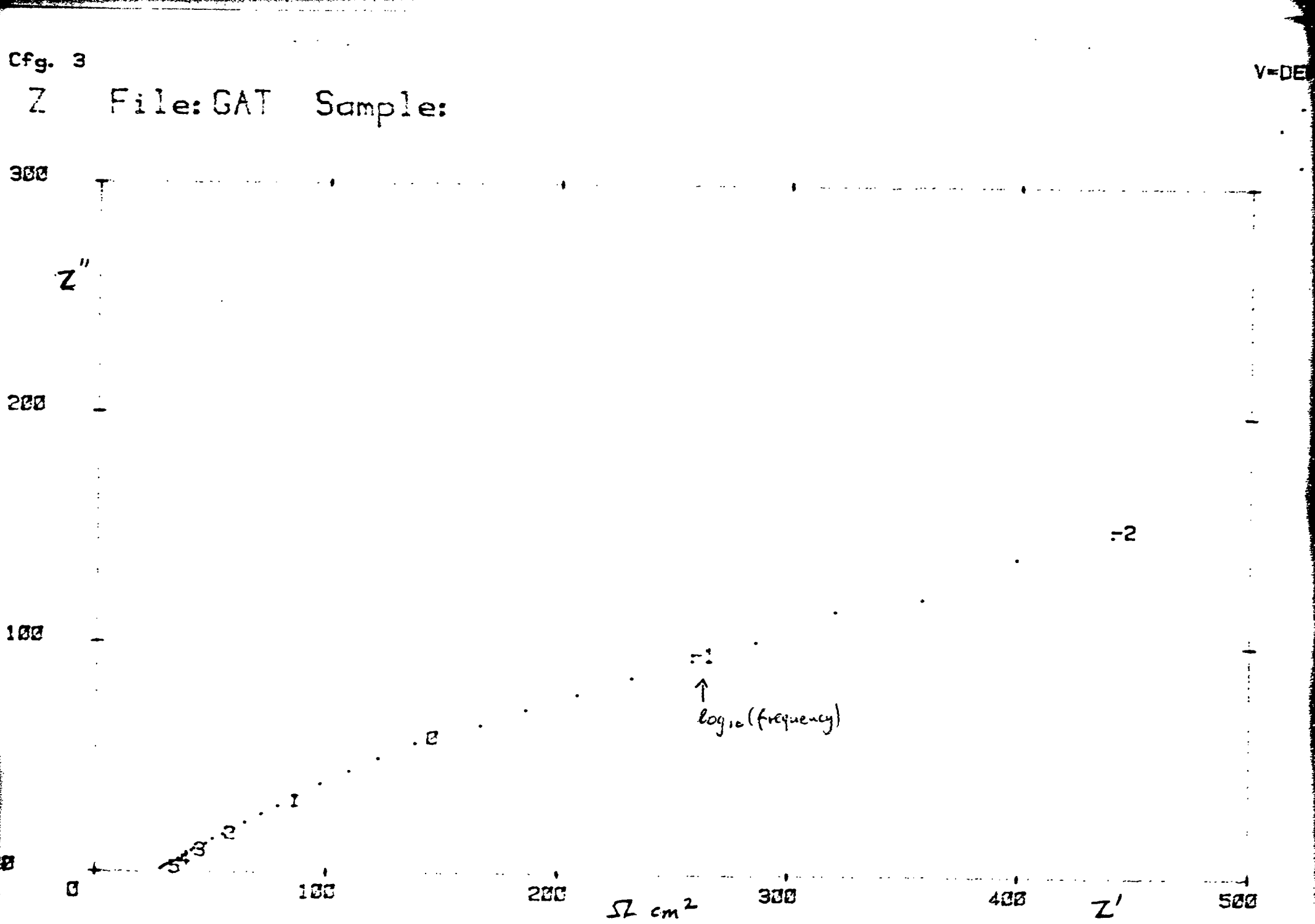

Fig. 16. Complex impedance due to LiAl composite.

Re-appraisal of negative plate materials

The energy density of an electrode material may be written:

$J = k.V.F.c$ where k is the efficiency of discharge
V is the average cell voltage
F is Faraday's constant
c is the concentration change of M^+ during discharge

c may be written in terms of a constant rate of change of the electrode potential with discharge:

$c = \Delta V(\frac{dE}{dc})^{-1}$ ΔV is the change in electrode potential, usually about 0.5 volt.

For a 2 volt cell, an energy density of the negative plate equal to 10KJ cm^{-3} (3 Whr cm^{-3}) can be obtained from a $(\frac{dE}{dc})$ value of 10 V cm^3 $mole^{-1}$. This value will be used as a typical figure for the calculation of power density.

The power density may be expressed in terms of the energy density:

$$W = \frac{\pi}{4} \cdot \frac{1}{k^2} \cdot \frac{\tilde{D}}{L^2} \cdot J$$

where L is the electrode thickness
$\tilde{D}$ is the diffusion coefficient

Therefore, at reasonable efficiencies, the factor $\frac{\tilde{D}}{L^2}$ determines the ratio of power density to energy density, and, accordingly, the approximate cycle period of the cell.

The diffusion coefficient is then required to be of the order of $10^{-8}cm^2sec^{-1}$ so that 0.1 millimeter thick electrodes can be discharged in four hours.

Using 10V cm^3 $mole^{-1}$ for the parameter $(\frac{dE}{dc})$ the values of $\tilde{D}^{\frac{1}{2}}$ $(\frac{dE}{dc})^{-1}$ given in section 2 may be converted into estimates of the diffusion coefficient. The estimates of $\tilde{D}$ fall in the range from $10^{-8}cm^2sec^{-1}$ for parts of the Hg/Li system to below $10^{-12}cm^2sec^{-1}$ for the glassy metal sample. The $FeSi_2$ sample was in the region of 10^{-9} to $10^{-10}cm^2sec^{-1}$. Only the Hg/Li system fulfilled the diffusion requirements, and in this case we had a very unfavourable energy density due to the high atomic weight of mercury.

The results of the analysis of composite electrodes indicated a solution to t' above problems. An ionically conducting additive can enhance the effective diffusion in a polycrystalline electrode compact according to the formula:

$$\tilde{D} \approx \frac{\sigma}{F} \left(\frac{dE}{dc}\right)$$

where σ is the effective ionic conductivity of the additive, allowing for tortuosity.

$\left(\frac{dE}{dc}\right)$ refers to the electrode component alone.

Using the same value as before for $\left(\frac{dE}{dc}\right)$ we obtain:

$$\tilde{D} \approx 10^{-4}\sigma$$

It must be remembered, however, that the addition of the ionic conductor dilutes the charge storage capacity and thus reduces the energy density. Typically, a 30% volume fraction of additive would reduce the energy density from 3 to 2 Whr cm^{-3}.

The polymer electrolyte may be seen as an effective additive; with its demonstrated conductivity of 5×10^{-4} $ohm^{-1}cm^{-1}$ we can expect the required diffusion coefficient of the composite to be $10^{-8}cm^2sec^{-1}$ with a tortuosity of 5. This estimate is on the pessimistic side a greater diffusion coefficient is obtained using a lower energy density. There is still a restriction on the diffusion coefficient of the electrode material. This is:

$$\tilde{D} > \frac{L^2}{t}$$

where L is the particle size
t is a time small compared with the discharge time.

Accordingly the particle size should be of the order of 10 micron and 1 micron for diffusion coefficients of 10^{-9} and $10^{-11}cm^2sec^{-1}$ respectively.

Another possibility for composite electrodes exists in a Li/Hg, Li/Al system. In this case the major component Li/Al would act as the charge storage medium and Li/Hg as the transporting agent. However, there is a strong possibility of inter-reaction of these phases which remains to be investigated. A complication arises with the Li/Hg additive due to the extreme variations in $D\left(\frac{dE}{dc}\right)^{-2}$, and therefore its ionic conductivity, with the electrode potential. The situations involving variable transport properties

have not yet been fully analysed, but a first conclusion is that fast transport at the extremities of electrode potential, at the expense of the diffusion properties of half-discharged material, would give a higher power density as well as a more constant voltage. This is indeed the case for the Li/Hg system (see fig 9)

In conclusion it may be said that a satisfactory negative plate material will probably be obtained in a composite of a suitable ionic conductor with a charge storage electrode, such as LiAl, in finely divided form. Using the parameters of known materials, an energy density of about 2whr cm^{-3} and a four hour discharge rate should be obtained from a 0.1mm thick electrode layer.

APPENDIX 1

SUMMATION OF CURRENTS DUE TO MANY POTENTIAL STEPS

(ANALYSIS BY T. GOODRICK, WOLFSON UNIT OF SOLID STATE IONICS)

Assumptions

① Constant value of $\frac{dE}{dc}$ – potential, E may be then expressed:

$$E = E_0 + \frac{dE}{dc} \cdot c$$

② semi-infinite sample

③ Constant diffusion coefficient, D

Transport equation

$$\frac{\partial c}{\partial t} = D \frac{\partial^2 c}{\partial x^2} \qquad \text{---- ①}$$

Boundary conditions

a) $c(x, t \leq 0) = 0$

b) $c(0, t) = c_1 \quad (0 < t \leq t_1)$

$= c_2 \quad (t_1 < t \leq t_2)$ etc

c) $\frac{\partial c}{\partial x}(\infty, t) = 0$

Solution Laplace transformation of ① gives:

$$\frac{d^2 \bar{c}}{dx^2}(x, p) - q^2 \bar{c}(x, p) = -\frac{c(x, t=0)}{D}$$

where $q^2 = p/D$

$$\therefore \frac{d^2 \bar{c}}{dx^2} - q^2 \bar{c} = 0 \quad \text{from (a)}$$

$\bar{c} = A e^{-qx}$ is a solution compatible with (c)

from (b). $\bar{c}(0, p) = \left. \frac{c_1 e^{-pt}}{-p} \right|_0^{t_1} + \left. \frac{c_2 e^{-pt}}{-p} \right|_{t_1}^{t_2} + \ldots$

$$= \frac{c_1}{p}(1 - e^{-pt_1}) + \frac{c_2}{p}\left[e^{-pt_1} - e^{-pt_2} \right] + \cdots$$

$$\bar{c}(0,p) = \frac{1}{p}\left[c_1 + (c_2 - c_1)e^{-pt_1} + (c_3 - c_2)e^{-pt_2} \cdots \right.$$

taking $\bar{c}_1(0,p) = \frac{c_1}{p}$

$$\bar{c}_1(x,p) = \frac{c_1 e^{-qx}}{p}$$

$$c_1(x,t) = c_1 \operatorname{erfc}\left(\frac{x}{2\sqrt{Dt}}\right)$$

$$\bar{c}(x,p) = \sum \bar{c}_i(x,p)$$

and $c(x,t) = \sum c_i(x,t)$

taking $\bar{c}_2(x,p) = \left(\frac{c_2 - c_1}{p}\right) e^{-qx} e^{-pt_1}$

inversion gives:

$$e^{-pt_1} = \int_0^\infty \delta(t - t_1) e^{-pt} dt \quad \text{for } t_1 > 0$$

The convolution theorem states:

for $\bar{c}(x,p) = \bar{f}_1(x,p)\bar{f}_2(x,p)$

$$c(x,t) = \int_0^t f_1(x,\tau) f_2(x, t-\tau)\, d\tau$$

So that $c_2(x,t) = \int_0^t (c_2 - c_1) \operatorname{erfc}\left(\frac{x}{2\sqrt{D(t-\tau)}}\right) \delta(\tau - t_1) d\tau$

$$= (c_2 - c_1) H(t - t_1) \operatorname{erfc}\left(\frac{x}{2\sqrt{D(t-t_1)}}\right)$$

(where $H(t) = \int_0^t \delta(\tau)\, d\tau$)

$$= \frac{(c_2 - c_1)}{c_1} H(t - t_1)\, c_1(t - t_1)$$

As $H(t-t_1) = 0$ for $t \leq t_1$, the 2nd term does not operate until $t > t_1$ where $H(t-t_1) = 1$

The solution is then:

$$c(x,t) = \sum_{n=0} \left[c_{n+1} - c_n \right] \operatorname{erfc}\left(\frac{x}{2\sqrt{D(t-t_n)}} \right) \cdot H(t-t_n)$$

where $c_0 - t_0 = 0$

The current density is:

$$I(t) = e J(t) = -e D \frac{\partial}{\partial x} c(0,t)$$

$$\frac{\partial}{\partial x} c_1(x,t) = -\frac{2}{\sqrt{\pi}} \left(\frac{c_1}{2\sqrt{Dt}} \right) e^{-x^2/4Dt}$$

$$\therefore \quad I_1 = e c_1 \sqrt{\frac{D}{\pi t}}$$

$$\text{and} \quad I(t) = e \sqrt{\frac{D}{\pi}} \sum_{n=0} \left[\frac{c_{n+1} - c_n}{\sqrt{t-t_n}} \right] H(t-t_n)$$